A fate-alternating transitional regime in contracting liquid filaments

F. Wang[1], F. P. Contò[1], N. Naz[1], J. R. Castrejón-Pita[1],
A. A. Castrejón-Pita[2], C. G. Bailey[1], W. Wang[1], J. J. Feng[3] and Y. Sui[1],†

[1]School of Engineering and Materials Science, Queen Mary University of London, London E1 4NS, UK

[2]Department of Engineering Science, University of Oxford, Oxford OX1 3PJ, UK

[3]Departments of Mathematics and Chemical and Biological Engineering, University of British Columbia, Vancouver, BC V6T 1Z2, Canada

The fate of a contracting liquid filament depends on the Ohnesorge number (Oh), the initial aspect ratio (Γ) and surface perturbation. Generally, it is believed that there exists a critical aspect ratio $\Gamma_c(Oh)$ such that longer filaments break up and shorter ones recoil into a single drop. Through computational and experimental studies, we report a transitional regime for filaments with a broad range of intermediate aspect ratios, where there exist multiple Γ_c thresholds at which a novel breakup mode alternates with no-break mode. We develop a simple model considering the superposition of capillary waves, which can predict the complicated new phase diagram. In this model, the breakup results from constructive interference between the capillary waves that originate from the ends of the filament.

Key words: capillary flows, drops

1. Introduction

The dynamics of contracting liquid filaments is a fundamental problem relevant to a wide range of natural phenomena and industrial applications (Eggers & Villermaux 2008; Driessen *et al.* 2013), from the breakup of ocean spume (Veron *et al.* 2012), ink-jet printing (Dong, Carr & Morris 2006; Xu & Basaran 2007; Wijshoff 2010) and spraying (Lefebvre & McDonell 2017) to microfluidics (Stone, Stroock & Ajdari 2004; Squires & Quake 2005) and particle technology (Hartnett *et al.* 2015). A number of computational and theoretical studies have considered Newtonian cylindrical free filaments that are initially stationary (Schulkes 1996; Notz & Basaran 2004; Driessen *et al.* 2013), as illustrated in figure 1. They conclude that the fate of the filament is controlled by the initial aspect ratio between the half filament length and its radius $\Gamma = L/R$, the Ohnesorge number ($Oh = \mu/\sqrt{\rho\sigma R}$, where μ, ρ and σ represent the viscosity, density of the filament and the surface tension coefficient, respectively),

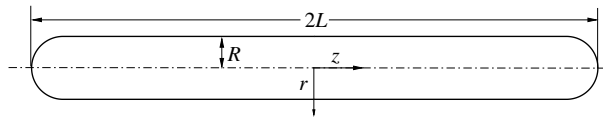† Email address for correspondence: y.sui@qmul.ac.uk

FIGURE 1. Illustration of the initial shape of a cylindrical filament. The length of the filament is $2L$ and the radii of both the cylindrical section and the semi-spherical ends are R. Cylindrical coordinates are defined at the centre of the filament.

which measures the relative importance of viscosity and surface tension, and the initial shape perturbation to the filament surface. Very viscous filaments ($Oh \gg 1$) have been found to be always stable (Eggers & Fontelos 2005; Castrejón-Pita, Castrejón-Pita & Hutchings 2012). Viscous filaments (i.e. $Oh \geqslant 0.1$) break up mainly due to the Rayleigh–Plateau instability (Driessen *et al.* 2013). Low-viscosity filaments can also fragment through the end-pinching mechanism: the contracting tip forms a blob connected to the central stationary filament. Due to surface tension, a neck forms in the connection region. The neck radius decreases towards zero, which breaks the blob from the filament, as described by Stone, Bentley & Leal (1986), Stone & Leal (1989), Schulkes (1996) and Notz & Basaran (2004).

So far it has been widely believed that for $Oh \leqslant 1$, at each Oh, there is a critical initial aspect ratio Γ_c at which a filament transits from no-break to breakup. In the present study, we revisit this classical problem using computational and experimental approaches. We mainly focus on low-viscosity filaments with $0.003 \leqslant Oh \leqslant 0.02$, seeking to establish the sequence of events when increasing the filament aspect ratio, and to understand the underlying mechanism that leads to the events.

2. Computational and experimental methods

In our numerical simulations, we consider axisymmetric liquid filaments surrounded by another fluid with negligible density and viscosity, as shown in figure 1, where the cylindrical coordinates are defined at the centre of the filament. Gravity is not considered. Both the filament and the ambient fluids are initially at rest; they are incompressible and Newtonian, so they are governed by the Navier–Stokes equations. Our numerical simulations consist of a finite volume method on a staggered grid, where a level-set method is used to capture the fluid interface. The code was developed by Sui & Spelt (2013, 2015). In the present study, we have checked for mesh convergence and domain independence to ensure that the reported results do not change with further increasing the mesh density or domain size.

Our experimental set-up is schematically shown in figure 2(*a*), and is adapted from a design described elsewhere (Castrejón-Pita *et al.* 2011). In brief, the jet generator consists of a long cylindrical chamber with an outlet nozzle of 2.29 mm in diameter in its lower side and closed at the top by a flexible rubber membrane mechanically coupled to an electromagnetic actuator (V201, LDS Instruments). The jet speed u ranges from 1.1 to 1.9 m s^{-1}. The jet is modulated by the electromagnetic actuator, driven by a harmonic waveform. The harmonic modulation produces a string of droplets by driving Rayleigh–Plateau instability on the jet surface; filaments can be formed between two droplets as secondary products of breakup, as shown in figure 2(*b*). The actuation frequency ν controls the droplet separation w, i.e. $\nu = u/w$, and consequently the length of the filament. At low modulation amplitudes, the jet breaks up at the front of the filament being formed, as shown in figure 2(*b*). This is
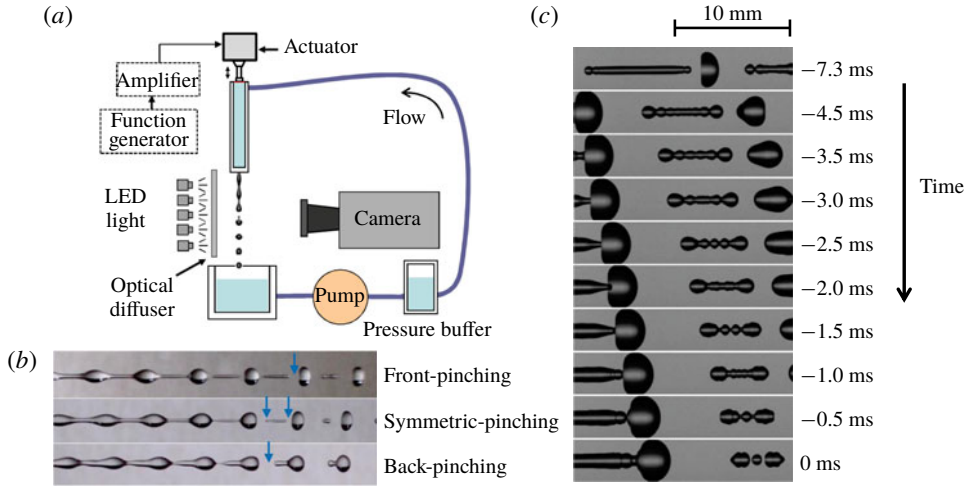
FIGURE 2. (Colour online) (*a*) Schematic of experimental set-up; (*b*) three modes of pinching in filament generation; (*c*) example of symmetric-pinching.

called front-pinching. At large modulation amplitudes, the jet breaks up at the back of the filament. This is called back-pinching. Symmetric filaments are produced by carefully adjusting the amplitude of the modulation to produce pinch-off at both ends simultaneously, and examples can be seen in figure 2(*c*). It is difficult to control the radius of the filament, which generally decreases with the filament length, but is also affected by the modulation amplitude. We conduct experiments with pure water at room temperature. The filament radius 0.15 mm $< R < 0.75$ mm is obtained by directly measuring the experimental images, and this gives $0.004 < Oh < 0.01$. Filaments are imaged by a high-speed camera (Phantom Miro, Phantom), with a macro lens (Tamron SP AF90) in shadowgraph configuration. Experiments are recorded at $20\,000$ frames per second with a 30 µs exposure. The region of interest is illuminated by a linear array of 10 W light-emitting diode (LED) lights, through an optical diffuser. Image resolution ranges from 12 to 32 pixels mm^{-1}. The present set-up permits a simpler control of the filament characteristics than the previous drop-on-demand mode set-up (Castrejón-Pita *et al.* 2012).

According to our calculations, the breakup behaviour of the liquid filaments is not expected to be influenced by the presence of air. Viscous drag from the surrounding air becomes significant for filaments with a radius smaller than $R\mu_{air}Oh^2/\mu$ (Chen, Notz & Basaran 2002). Under our conditions, this critical radius is far below the resolution of the imaging system. Inertial influences from air would become significant when the air Weber number, $We_{air} = \rho_{air}u^2R/\sigma$, exceeds 0.2 (van Hoeve *et al.* 2010). In our work, We_{air} is always less than 0.07. In the experiments, a filament contracts under surface tension effect during its free fall. The importance of gravity compared with surface tension can be estimated by comparing the capillary velocity u_c to the velocity increase of the filament due to gravity during one acoustic period Δu_g. The capillary velocity $u_c = R/t_i$, where $t_i = \sqrt{\rho R^3/\sigma}$ is the inertial-capillary time; Δu_g can be approximated by gw/u. If we use typical values of $R = 0.5$ mm, $u = 1$ m s^{-1} and $w = 0.01$ m, the value of $u_c/\Delta u_g$ is ∼4, indicating that gravity may not significantly affect the filament fate. The conclusion seems to be confirmed by the good agreement
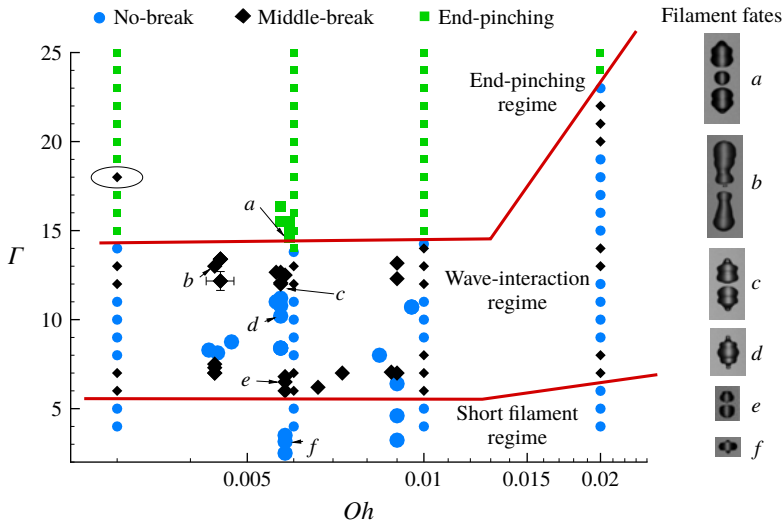
FIGURE 3. (Colour online) Fates of filaments with different initial aspect ratios and Ohnesorge numbers. Small solid symbols are results from numerical simulations. Large solid symbols represent experiments; many of them correspond within error bars to simulations (typical error bars are shown near photo inset *b*). Photo insets on the right show fates of the filaments. Two solid lines (red online) are used as guides for the eyes to divide regimes. Right above the upper line the filament breaks into three parts through end-pinching (a special case for $\Gamma = 18$ at $Oh = 0.003$ is highlighted by an oval and is discussed in §3.2), between the two lines the filament shows alternate middle-break and no-break and below the lower line the filament is too short to break.

between numerical simulations and experiments in terms of the filament fates and the contracting dynamics shown in §3.1. The numerical simulations have omitted gravity.

We have limited our studies to low-viscosity filaments with $0.003 \leqslant Oh \leqslant 0.02$, mainly because of the limitations of the present computational and experimental methods. Our numerical simulation becomes increasingly unstable with even lower Oh. At higher Oh, i.e. $Oh = 0.04$, a much higher aspect ratio (typically $\Gamma > 50$) is required to observe filament end-pinching. It is experimentally difficult to generate a symmetric long filament with the present method. The computational time also increases significantly when viscous effect becomes significant.

3. Results and discussion

3.1. *Phase diagram*

Figure 3 summarizes the fate of the filament as a function of the initial aspect ratios Γ and Ohnesorge number Oh. Note that the phase diagram has focused on the low-viscosity phase space ($Oh < 0.02$), where the dominant mechanism for breakup of initially smooth filaments has been found to be end-pinching, i.e. the contracting bulbous ends break from the central filament. From the phase diagram, we can see that contrary to the present understanding that at each Oh there exists one critical Γ_c which divides no-break and breakup regimes, the present computational and experimental results clearly show that there is a transitional regime for filaments in a broad range of intermediate Γ, where there are multiple Γ_c at which the filament
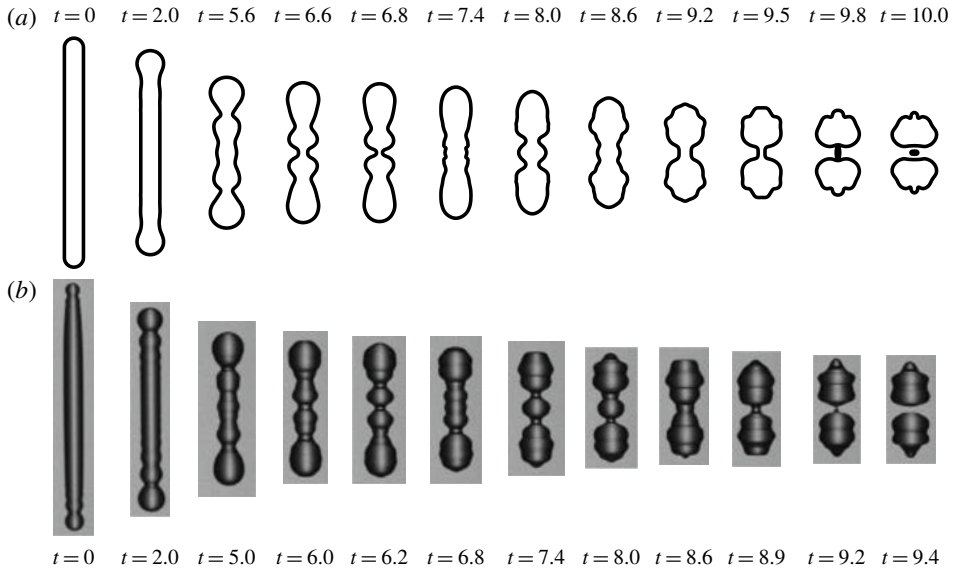
FIGURE 4. Instantaneous profiles of a contracting filament from numerical simulation (*a*) and experiment (*b*). Parameters are $Oh = 0.0057$, $\Gamma = 12$.

alternates between no-break and a novel middle-break mode. After breakup, the two parts can have a moderate aspect ratio (inset *c*) or an elongated filamentous shape (inset *b*).

Notz & Basaran (2004) first discovered a third regime between end-pinching and no-break, where a filament breaks after shape oscillations. However, they did not observe the fate alternation and the middle-break mode in their numerical study. The present phase diagram has three regimes, separated by the two solid lines (red online) in figure 3. For long filaments (large Γ), breakup happens through the end-pinching mechanism where droplets break from the filament at the contracting ends. Photo inset *a* in figure 3 shows a case right above the lower boundary of end-pinching; the size of the filament between the two droplets will increase with Γ. For short filaments, the contraction time is too short for any capillary instability to develop and therefore a filament contracts to a droplet. Both regimes have been well documented previously (Stone *et al.* 1986; Stone & Leal 1989; Schulkes 1996; Notz & Basaran 2004; Castrejón-Pita *et al.* 2012). In the fate-alternating transitional regime between end-pinching and short-filament regimes, we observe strong wave interactions on the filament surface and therefore name it the wave-interaction regime. Also note the peculiar case of a filament with $\Gamma = 18$ at $Oh = 0.003$, which breaks into two filaments from the middle within the end-pinching regime where filaments first break into three parts. As we shall see later, this isolated case is explained by the same mechanism that explains the fate-alternating transitional regime.

An overview of the filament contraction in the wave-interaction regime is presented in figure 4 for a filament with $\Gamma = 12$ at $Oh = 0.0057$, which is the same case as the photo inset *c* in figure 3 where the filament breaks from the middle into two droplets. In figure 4 we also compare the instantaneous profiles from the numerical simulation and experiment. It should be noted that in experiments a filament is generated between two droplets as a secondary product of breakup. Therefore when

the filament evolves into a cylindrical shape with semi-spherical ends, it already has a non-negligible contracting speed, which leads to faster filament contraction and wave evolution at the early stage, compared with numerical simulations where the filament is initially stationary. This can be seen from the comparison at $t = 2.0$. However, the evolution of the filament at a later stage ($t \geqslant 5.0$) seems to have not been affected too much by the initial differences. The filament profiles from numerical simulation agree reasonably well with experiments, with a single adjustment of the time by 0.6. Note here the time is made dimensionless by the inertial-capillary time t_i. From figure 4 we can see waves propagate inwards with the contracting ends and interact at the middle plane. From the experimental images, when the experimental time is around $t = 6.0$ the secondary troughs from both ends meet at the middle plane to form a neck which, however, is not deep enough to break the filament. The neck reopens, followed by the collision of the two primary troughs associated with the bulbous ends, at the experimental time of around $t = 8.6$. The neck formed is deep enough to trigger thinning which finally leads to breakup.

3.2. *Capillary wave superposition: a simple model to predict filament fate*

We investigate the underlying mechanism that leads to the non-uniqueness of Γ_c and the novel middle-break mode. We find that for a filament with an intermediate Γ, the interactions of capillary waves originating from both ends determine the filament fate. It is difficult to analyse the wave interactions directly on filaments of intermediate Γ, as the waves emanating from both ends quickly superimpose after the onset of contraction, and become impossible to disentangle and track individually. Instead, we first investigate the propagation of such capillary waves on a long filament, without wave interaction. We superpose the waves that we obtained from the long filament onto a shorter filament to determine how the waves interact on the latter and potentially cause breakup.

As an example of capillary waves without interaction, we examine the filament with $\Gamma = 25$ at $Oh = 0.01$, which eventually breaks up through end-pinching. Figure 5(*a*) shows the propagation of capillary waves from the contracting tip towards the centre of the filament. The peaks and troughs of the waves are numbered. The mechanism of the generation of the capillary waves is similar to that of a contracting two-dimensional liquid sheet studied by Song & Tryggvason (1999), and may be understood by examining the vorticity near the contracting tip of the filament, which is shown in figure 6. In the early contraction of the bulbous end and the associated trough T1, due to the variation of the sign of their axial curvature, primary vorticity with positive sign is formed near the bulbous region; secondary negative vorticity develops at the neck of T1 (see figure 6*a*). Due to low viscous diffusion, in the region below the trough T1 where the axial curvature is positive, tertiary positive vorticity forms and causes the development of the secondary bulb and the secondary necking (see figure 6*b*). The process repeats and forms a series of waves towards the middle plane $z = 0$ as shown in figure 6(*c*).

In figure 5(*a*), the amplitude of a wave peak or trough is defined as $a(t) = r(t) - R$, where $r(t)$ is the instantaneous filament radius at the peak or trough. Quantities are made non-dimensional by the initial filament radius R, the inertial-capillary time t_i and the Taylor–Culick capillary speed R/t_i (Keller 1983; Keller, King & Ting 1995). The time evolutions of the amplitudes of the wave peaks and troughs and their z-axis positions are plotted in figure 5(*b*). We can see that the amplitudes oscillate before end-pinching takes place. For example, the filament neck (i.e. T1)
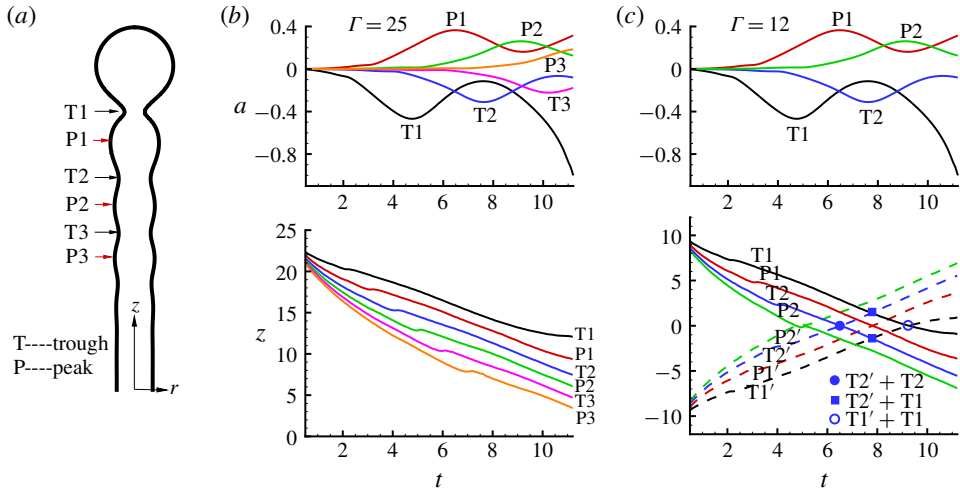
FIGURE 5. (Colour online) (*a*) Definitions of capillary waves on a contracting filament. (*b*) Amplitudes (upper) and axial positions (lower) of wave troughs and peaks on a contracting filament with $\Gamma = 25$ at $Oh = 0.01$ from numerical simulation. Panel (*c*) is for $\Gamma = 12$ and is mapped from (*b*) as explained in the text. The dashed lines in (*c*) are waves from the opposite ends of the filament. Note that the present model assumes that the capillary waves pass each other unchanged, unless two troughs would produce a thin neck that could break the filament.
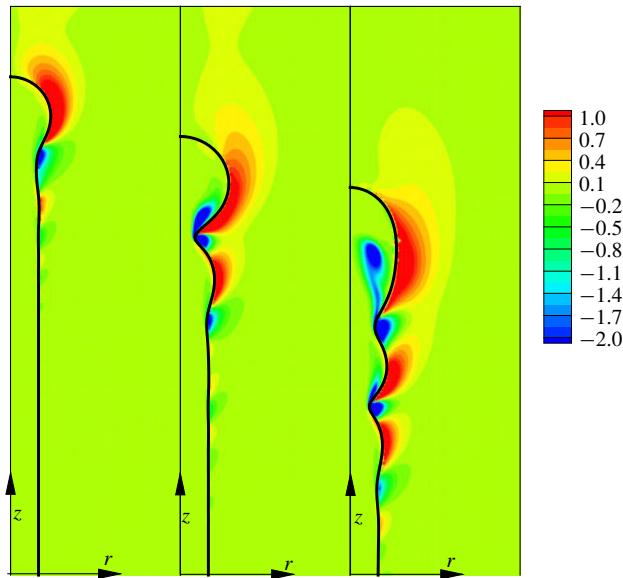

FIGURE 6. (Colour online) Temporal evolution of the vorticity contours near the contracting end of a filament with $\Gamma = 25$ at $Oh = 0.01$. Only a quarter of the domain is shown.

initially decreases and then reopens before its final decreasing to -1. This indirect end-pinching, contrasting to direct end-pinching (for filaments with very low viscosity) where T1 decreases to -1 monotonically, has been documented by Hoepffner & Paré

(2013). The wave peaks and troughs travel at an almost constant speed ($\sim$1.05 for all present cases) except at the very early stage of filament contraction when the waves are being generated. This suggests that the relative distances between adjacent peaks or troughs (i.e. wavelength) largely remain unchanged ($\sim$3) and the phases of the waves are stationary with respect to the contracting ends. It should be noted that self-similar waves generated in the retraction of liquid cones have been previously analysed (Sierou & Lister 2004). However, the present waves cannot be described by the self-similar solutions, due to geometric differences.

We propose a simple model that predicts the fate of a filament of intermediate aspect ratio from the superposition of capillary waves emanating from both ends. In this model, we assume that the capillary waves of figure 5(b) will travel inward from both ends, and that they will interact linearly upon collision. When two troughs Ti and Tj meet, in particular, they produce a deeper trough of amplitude $a_{Ti} + a_{Tj}$. As an example, figure 5(c) plots the trajectories of the first two troughs and peaks from each end of a filament with $\Gamma = 12$, shifted from those of figure 5(b) towards $z = 0$ by the difference in their Γ. The circular and square symbols mark where two troughs meet to produce a deeper trough. The model asserts that if its amplitude exceeds a threshold, the filament will break due to capillary instability. When analysing filaments at a different Oh, one must use the long-filament waves for that Oh value. Hoepffner & Paré (2013) tracked the time evolution of the radius of T1; however, their model does not account for wave interaction which is central to the filament fate in the transitional wave-interaction regime.

The threshold can be estimated from a simple scaling argument. When two wave troughs on the filament approach each other, whether they break the filament after superposition or not depends on two competing time scales: the breakup time of the superposed trough and the meeting time of the two waves. For the present cases, since both waves travel at a speed of about 1.05, the meeting time can be estimated by $t_m = \lambda/(1.05 \times 2)$, where λ is the wavelength and is $\simeq 3$ from present simulations. We can estimate the breakup time from the fastest growing mode of the Rayleigh–Plateau instability; then $t_b = (1/\omega_{max})\ln(1/-b)$, where ω_{max} is the fastest wave growth rate and is readily available from the literature (Weber 1931). The term b is the superposed trough amplitude (i.e. $a_{Ti} + a_{Tj}$), and its value is used as the initial perturbation amplitude in the Rayleigh–Plateau instability. The filament would break when $t_b < t_m$, and that leads to the critical superposed trough amplitude $b_c = -1/\exp(\lambda\omega_{max}/2.1)$. With Oh ranging from 0.003 to 0.02, b_c is between -0.616 and -0.605. For simplicity, a threshold of -0.61 is used in the present model. Note that the above estimation applies linear results to waves of finite amplitudes, which violates mass conservation by an amount that is proportional to the square of amplitude. Linearizing the disturbance in the cross-sectional area will be more accurate, but is perhaps also more complicated.

The fates of filaments predicted by the simple wave superposition model are presented in figure 7, together with the full-simulation and available experimental results. The boundaries between different modes are represented by solid and dashed lines in the phase diagram: solid lines divide the three different regimes, and dashed lines separate middle-break and no-break modes in the wave-interaction regime. It can be seen that the simple model can predict almost all the outcomes in the phase diagram and define the whole phase space.

Next we demonstrate how the simple model can predict the fates of the filaments and define the whole phase space. Figure 8 examines the interactions of capillary waves on six filaments of decreasing Γ, at $Oh = 0.01$, corresponding to distinct
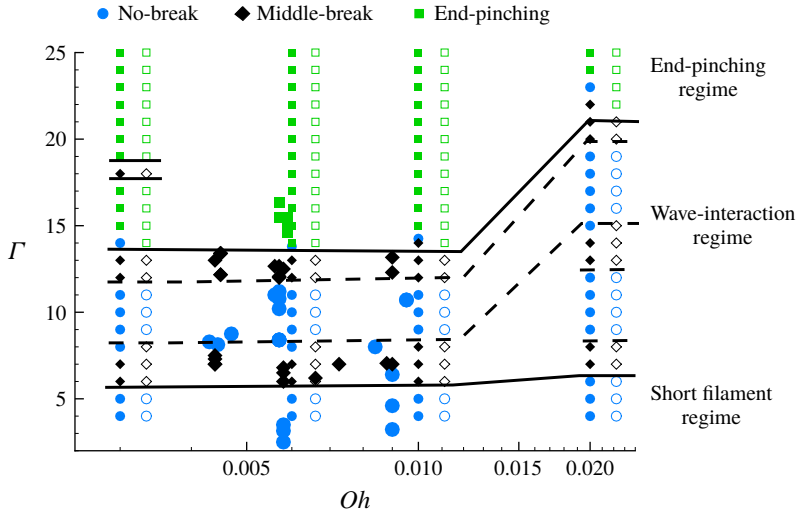
FIGURE 7. (Colour online) The same phase diagram of filaments as in figure 3 with predictions from the simple wave superposition model. Small solid symbols are from numerical simulations; open symbols on the right are results at the same Oh and are from the simple model. Large solid symbols represent experiments. The solid and dashed lines are phase boundaries predicted by the simple model. Solid lines divide the three regimes; dashed lines separate middle-break and no-break modes in the wave-interaction regime.

breakup scenarios in figure 3. In almost all cases that we have considered, the breakup only involves the first two troughs, T1 and T2, and we will focus on these at present. Figure 8(a) demonstrates the 'classical' end-pinching scenario for $\Gamma = 25$, with the trough T1 attaining $a = -1$ in time before any significant wave interaction. Thus, the filament breaks up into three parts as shown in the inset. On shorter filaments, the end-pinching occurs closer to the mid-point ($z = 0$). A threshold is when T1 attains $a = -1$ right at $z = 0$. This happens for $\Gamma = 13.4$, and marks the transition to the wave-interaction regime.

In the wave-interaction regime, a subtlety is that it is not known *a priori* which troughs would superimpose to produce a neck that leads to breakup. The troughs closer to the middle meet sooner, but their amplitudes tend to be smaller, and this may or may not produce necking. Besides, the amplitudes vary in time as well (figure 8a). These open up the possibility of a non-monotonic dependence of pinch-off behaviour on Γ. As demonstrated below, the simple model can predict the phase space and the fates of the filaments.

In figure 8, we mark the time when the amplitude of the trough T1 crosses -0.305 (a linearly superposed amplitude of the new trough from T1 + T1′ collision will therefore be at the breakup threshold of -0.61). From the time evolution of the amplitude of trough T1 in the upper panel of figure 8(a), we can expect that if the trough T1 of a filament arrives at $z = 0$ between t_1 and t_2 or after t_3, the filament will break up from the middle. Since the time it takes for a trough to reach $z = 0$ depends on the filament length and can be predicted by the simple model (through mapping the waves of a long filament to shorter filaments), we can expect that there are two windows of Γ in the wave-interaction regime where the filament breaks from the middle. This is consistent with the full numerical simulations and the experiments as shown in figure 7.
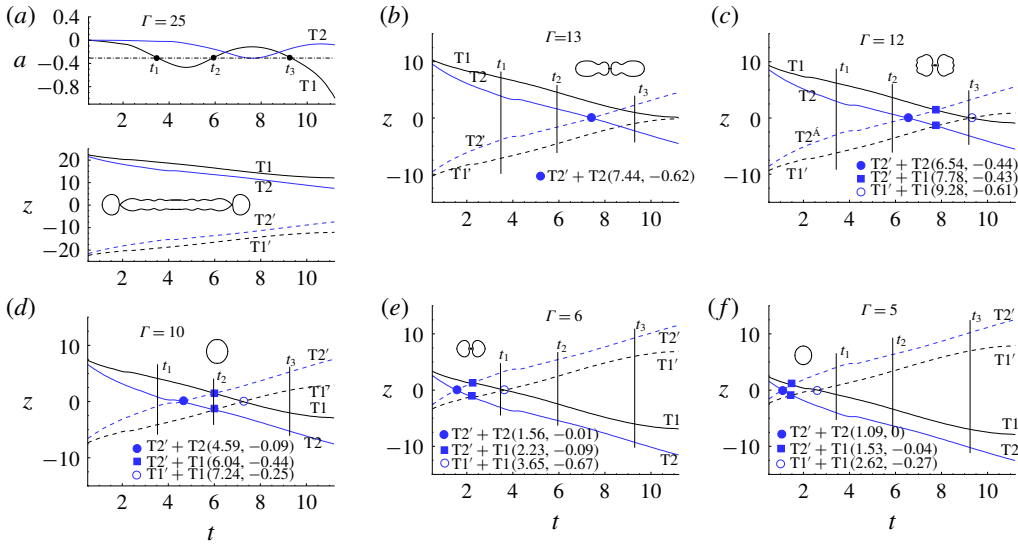
FIGURE 8. (Colour online) Amplitudes (upper panel in (*a*)) and axial positions of wave troughs on contracting filaments with decreasing Γ at $Oh = 0.01$. In (*a*) the three dots mark the time when the amplitude of the trough T1 crosses -0.305 (a linearly superposed amplitude of the new trough from T1 $+$ T1' collision will be at the breakup threshold of -0.61). The three time instances are labelled as vertical solid lines in (*b–f*). If the trough T1 arrives at $z = 0$ between t_1 and t_2 or after t_3, the linearly superposed amplitude of the new trough from T1 $+$ T1' collision will be above the threshold and the filament will break up from the middle. Results are obtained by mapping the waves on a long filament with $\Gamma = 25$ (from numerical simulation) to shorter filaments in the same manner as in figure 5. The circular and square symbols (blue online) mark collisions between troughs, and the two numbers in the legend are the time of collision and the resultant amplitude from linear superposition, respectively. The insets are numerical results showing the fates of the filaments.

From figure 8(*a*), we can also see that in a very short time interval around $t = 7.5$, the amplitude of trough T2 is below -0.305, suggesting a small window of Γ where the filament will break in the middle due to the T2 $+$ T2' collision. Such an example is shown in figure 8(*b*) for a filament with $\Gamma = 13$, which breaks after the collision between T2 and T2' at $t = 7.44$. This happens before other potential interactions of T1 $+$ T2' or T1 $+$ T1'.

On the shorter filament of figure 8(*c*), the collision T2 $+$ T2' occurs sooner than in figure 8(*b*), but the trough is shallower. Thus, this collision does not produce breakup, nor do the subsequent collisions of T1 $+$ T2' and T1' $+$ T2. Eventually, the T1 $+$ T1' collision after t_3 at $t = 9.28$ produces a deep enough trough that splits the filament into two. In figure 8(*b,c*), the wave superposition model accurately predicts the outcome of the breakup, shown as insets. Besides, note that the T2 $+$ T2' collision breaks the filament into two short filaments (figure 8*b*) while the T1 $+$ T1' collision leads to two drops (figure 8*c*). Those roughly correspond with the experimental images of insets *b* and *c* in figure 3, the differing shapes being readily explained by the different troughs involved in the breakup.

With decreasing Γ, the collision scenarios are similar to figure 8(*c*) except that the T1 $+$ T1' collision occurs sooner when T1 has a shallower amplitude (see the time
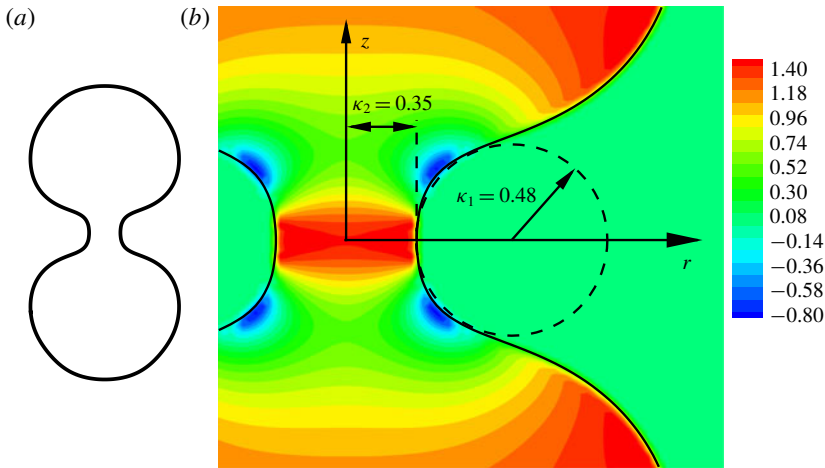
FIGURE 9. (Colour online) (*a*) Profile of the filament with $\Gamma = 6$ at $Oh = 0.01$ when the troughs T1 and T1′ meet at the middle plane $z = 0$. (*b*) Amplified neck region of the filament in (*a*) with pressure contours. Here κ_1 and κ_2 measure the radius of curvature in r–z and azimuthal planes, respectively.

evolution of wave amplitudes in figure 8*a*). When the trough T1 of a filament reaches $z = 0$ between the time t_2 and t_3, the linearly superposed amplitude from the T1 + T1′ collision will be smaller than the threshold, leading to no breakup. An example is shown by a filament with $\Gamma = 10$ (figure 8*d*). The critical Γ_c dividing the middle-break and no-break regimes is represented by the upper dashed line at $Oh = 0.01$ in figure 7. It corresponds to the filament whose trough T1 reaches $z = 0$ at the time t_3.

For even shorter filaments, their trough T1 can reach the middle plane before time t_2, then the T1 + T1′ collision can generate a trough that is strong enough and results in breakup, as shown by the filament with $\Gamma = 6$ (figure 8*e*).

Finally, the troughs of short filaments such as $\Gamma = 5$ (figure 8*f*) reach the middle plane $z = 0$ too soon (i.e. before t_1) for any trough superposition to be sufficiently deep. In the phase diagram the point of $\Gamma = 5$ falls below the phase boundary dividing the middle-break and short-filament no-break regimes (the lower black solid line in figure 7). The phase boundary is obtained by identifying the critical Γ_c where the trough T1 of the filament reaches $z = 0$ at the time t_1. Overall, figure 8 suggests that the simple model has captured all the noted outcomes in the phase diagram and can define the whole phase space.

In our simple model, we have assumed that the Rayleigh–Plateau type of necking will happen and lead to breakup if two troughs meet and the linearly superimposed trough amplitude is larger than a threshold. It is interesting to study the filament profile when two troughs meet. Figure 9 presents the filament profile and the pressure contour at $t = 3.65$ when T1 and T1′ meet at $z = 0$, for the filament shown in figure 8(*e*) which breaks after the trough collision. It is clearly seen that the radius of the azimuthal curvature is smaller than that of the axial curvature which has an opposite sign due the shape of the trough. This results in a positive Laplace pressure which drives liquid away from the neck, finally leading to breakup. A similar phenomenon is observed for the filaments in figure 8(*b*,*c*), at the instances of trough collision leading to middle-break. For the filament shown in figure 9, we notice that

without trough collision, the Laplace pressure inside the trough T1 will be negative at $t = 3.65$, because the radius of the azimuthal curvature would not be small enough.

Now we turn to the special case of $\Gamma = 18$ and $Oh = 0.003$ in figure 3, where the filament breaks up in the middle into two short filaments, whereas longer and shorter filaments both exhibit end-pinching. This case is peculiar in that before the trough T1 produces end-pinching, the troughs T3 and T3′ meet at $z = 0$, producing a trough just deep enough to split the filament into two. On a longer filament, T1 will have attained $a = -1$ before the T3 + T3′ collision, thus producing classical end-pinching. On shorter filaments, the troughs T3 and T3′ are not deep enough when they meet, but the filament contraction time is still sufficiently long to allow T1 to produce end-pinching.

3.3. *Limitations of the wave superposition model*

We note the failure of the wave superposition model in capturing the outcome of filaments just below the upper solid red line in figure 3. For three out of the four Oh values tested, the model suggests end-pinching while numerical simulations produce no-break or middle-break. The model assumes that the capillary waves pass each other unchanged, unless two troughs would produce a thin neck that could pinch off within the meeting time. This is not quite true for those few filaments where, shortly before end-pinching, the trough T1 meets the strong peak P1′. The peak P1′ opens the neck of T1 to some extent, which leads to no-break or middle-break.

A second major limitation of the model is that it is not entirely self-contained. At each Oh, one will need to first obtain the evolution of non-interacting waves from full numerical simulation of a long filament at the same Oh. The fates of shorter filaments can then be predicted by mapping the waves to shorter filaments and analysing their interactions. The main difficulty of developing a full predictive model lies in the fact that the wave amplitudes oscillate in time in a complicated way and building a mechanistic model to explicitly describe the oscillation is non-trivial. Finally, the present study is limited to low-viscosity filaments. The performance of the simple model on more viscous filaments is yet to be tested.

4. Concluding remarks

To summarize, we find that for a contracting filament with low viscosity, end-pinching happens only when the filament is sufficiently long. For filaments with intermediate lengths, the contraction time is too short for the neck to develop to end-pinching, and a filament's fate will be decided by the interactions of capillary waves. The amplitudes of the waves oscillate in time, leading to alternate no-break and middle-break modes of the filament with increasing length. Short filaments will not break because of the short contraction time.

The fate-alternating transitional regime and the middle-break mode are the new findings of this work. They show the importance of the superposition of capillary waves, which can serve as a new mechanism for controlling the breakup of liquid filaments. The simple but effective wave superposition model proposed here may be applicable to other systems, such as the ejection of small droplets in rapid droplet spreading (Ding *et al.* 2012). Towards practical applications, the broad transitional regime offers new means to control and manipulate the integrity and breakup of filaments of a wide range of lengths. The novel middle-break mode also provides a new mechanism to generate equal-sized small droplets. Both can potentially improve the current design strategies in technologies such as ink-jet printing.

Acknowledgements

REFERENCES

CASTREJÓN-PITA, A. A., CASTREJÓN-PITA, J. R. & HUTCHINGS, I. M. 2012 Breakup of liquid filaments. *Phys. Rev. Lett.* **108** (7), 074506.

CASTREJÓN-PITA, J. R., MORRISON, N. F., HARLEN, O. G., MARTIN, G. D. & HUTCHINGS, I. M. 2011 Experiments and Lagrangian simulations on the formation of droplets in drop-on-demand mode. *Phys. Rev.* E **83** (3), 036306.

CHEN, A. U., NOTZ, P. K. & BASARAN, O. A. 2002 Computational and experimental analysis of pinch-off and scaling. *Phys. Rev. Lett.* **88** (17), 174501.

DING, H., LI, E. Q., ZHANG, F. H., SUI, Y., SPELT, P. D. M. & THORODDSEN, S. T. 2012 Propagation of capillary waves and ejection of small droplets in rapid droplet spreading. *J. Fluid Mech.* **697**, 92–114.

DONG, H., CARR, W. W. & MORRIS, J. F. 2006 An experimental study of drop-on-demand drop formation. *Phys. Fluids* **18** (7), 072102.

DRIESSEN, T., JEURISSEN, R., WIJSHOFF, H., TOSCHI, F. & LOHSE, D. 2013 Stability of viscous long liquid filaments. *Phys. Fluids* **25** (6), 062109.

EGGERS, J. & FONTELOS, M. A. 2005 Isolated inertialess drops cannot break up. *J. Fluid Mech.* **530**, 177–180.

EGGERS, J. & VILLERMAUX, E. 2008 Physics of liquid jets. *Rep. Prog. Phys.* **71** (3), 036601.

HARTNETT, C. A., MAHADY, K., FOWLKES, J. D., AFKHAMI, S., KONDIC, L. & RACK, P. D. 2015 Instability of nano- and microscale liquid metal filaments: transition from single droplet collapse to multidroplet breakup. *Langmuir* **31** (50), 13609–13617.

HOEPFFNER, J. & PARÉ, G. 2013 Recoil of a liquid filament: escape from pinch-off through creation of a vortex ring. *J. Fluid Mech.* **734**, 183–197.

VAN HOEVE, W., GEKLE, S., SNOEIJER, J. H., VERSLUIS, M., BRENNER, M. P. & LOHSE, D. 2010 Breakup of diminutive Rayleigh jets. *Phys. Fluids* **22** (12), 122003.

KELLER, J. B. 1983 Breaking of liquid films and threads. *Phys. Fluids* **26** (12), 3451–3453.

KELLER, J. B., KING, A. & TING, L. 1995 Blob formation. *Phys. Fluids* **7** (1), 226–228.

LEFEBVRE, A. H. & MCDONELL, V. G. 2017 *Atomization and Sprays*. CRC Press.

NOTZ, P. K. & BASARAN, O. A. 2004 Dynamics and breakup of a contracting liquid filament. *J. Fluid Mech.* **512**, 223–256.

SCHULKES, R. M. S. M. 1996 The contraction of liquid filaments. *J. Fluid Mech.* **309**, 277–300.

SIEROU, A. & LISTER, J. R. 2004 Self-similar recoil of inviscid drops. *Phys. Fluids* **16** (5), 1379–1394.

SONG, M. & TRYGGVASON, G. 1999 The formation of thick borders on an initially stationary fluid sheet. *Phys. Fluids* **11** (9), 2487–2493.

SQUIRES, T. M. & QUAKE, S. R. 2005 Microfluidics: fluid physics at the nanoliter scale. *Rev. Mod. Phys.* **77** (3), 977–1026.

STONE, H. A., BENTLEY, B. J. & LEAL, L. G. 1986 Experimental study of transient effects in the breakup of viscous drops. *J. Fluid Mech.* **173** (1), 131–158.

STONE, H. A. & LEAL, L. G. 1989 Relaxation and breakup of an initially extended drop in an otherwise quiescent fluid. *J. Fluid Mech.* **198**, 399–427.

STONE, H. A., STROOCK, A. D. & AJDARI, A. 2004 Engineering flows in small devices: microfluidics toward a lab-on-a-chip. *Annu. Rev. Fluid Mech.* **36**, 381–411.

SUI, Y. & SPELT, P. D. M. 2013 Validation and modification of asymptotic analysis of slow and rapid droplet spreading by numerical simulation. *J. Fluid Mech.* **715**, 283–313.

SUI, Y. & SPELT, P. D. M. 2015 Non-isothermal droplet spreading/dewetting and its reversal. *J. Fluid Mech.* **776**, 74–95.

VERON, F., HOPKINS, C., HARRISON, E. L. & MUELLER, J. A. 2012 Sea spray spume droplet production in high wind speeds. *Geophys. Res. Lett.* **39** (16), L16602.

WEBER, C. 1931 Zum zerfall eines flüssigkeitsstrahles. *Z. Angew. Math. Mech.* **11** (2), 136–154.

WIJSHOFF, H. 2010 The dynamics of the piezo inkjet printhead operation. *Phys. Rep.* **491** (4–5), 77–177.

XU, Q. & BASARAN, O. A. 2007 Computational analysis of drop-on-demand drop formation. *Phys. Fluids* **19** (10), 102111.